

# Photovoltaic Properties and Negative Capacitance Spectroscopy of PCBM:P3HT/FTO Nanostructured Counter Electrode for TiO<sub>2</sub>-Based DSSC

I. S. Yahia · Sh. A. Mansour · Hoda S. Hafez ·  
K. Ocakoglu · F. Yakuphanoglu

Received: 4 June 2012 / Accepted: 25 July 2012  
© Springer Science+Business Media, LLC 2012

**Abstract** Nano-clusters blind films of phenyl C61-butyric acid methyl ester (PCBM) and poly(3-hexylthiophene) (P3HT) were deposited on fluorine doped tin-oxide (FTO) substrate by spin coating and applied as counter electrodes instead of platinum for a new FTO/TiO<sub>2</sub> + K30 dye-sensitized solar cell. The photovoltaic parameters of the fabricated solar cell; open circuit voltage, short circuit current, output power and fill factor, were studied under various light intensities in the range 20:110 mW cm<sup>-2</sup>. An impedance spectroscopy study was also performed in a wide frequency range (5 kHz–1 MHz) to study the electron transport properties of the solar cells. The capacitance–voltage of the prepared DSSC is characterized by two parts: positive values of capacitance at low frequency

range,  $f \leq 100$  kHz and negative capacitance i.e., an inductive behavior, in higher frequency range  $f \geq 300$  kHz. Conducting polymer electrode based on PCBM:P3HT/FTO can be used as a counter electrode in a DSSC.

**Keywords** DSSC · PCBM:P3HT · K30 dye · Photovoltaic properties · Impedance spectroscopy · Negative capacitance

## 1 Introduction

In the past two decades, considerable efforts have been devoted to study the dye-sensitized nanocrystalline solar cell (DSSCs), since its first prototype was reported by O'Regan and Grätzel [1]. DSSCs have attracted much attention because of their low cost, possible fabrications of flexible devices, and relatively efficient devices for the photovoltaic conversion of solar energy [2, 3]. In development of DSSCs, key challenges include the demonstration of high efficiency and scale-up of fabrication. As the conventional counter electrode material in DSSC, platinum (Pt) is a burden for large-scale applications of DSSCs because it is one of the most expensive materials available [4]. As be known that, the common methods to deposited Pt thin films on a transparent conductive glass substrate to be used as counter electrodes are vacuum vapor deposition and sputtering which are very expensive methods [5]. Furthermore, the size of the substrate was limited, so it is hard to form a Pt layer on the large area substrate. Recently, in order to reduce the production cost of DSSC, conducting polymers are applied in counter electrode materials to replace platinized electrode [6, 7].

The counter electrode in DSSCs promotes the electron translocation from the external circuit back to the redox

---

I. S. Yahia  
Nano-Science & Semiconductor Labs., Physics Department,  
Faculty of Education, Ain Shams University, Roxy, Cairo, Egypt

Sh. A. Mansour (✉) · F. Yakuphanoglu  
Physics Department, Faculty of Science,  
Firat University, Elazig, Turkey  
e-mail: shehab\_mansour@yahoo.com

Sh. A. Mansour  
Basic Engineering Science Department, Faculty of Engineering,  
Menofia University, Shebin El-Kom, Egypt

H. S. Hafez  
Nano-Photochemistry and its Environmental Applications  
Laboratory, Environmental Studies and Research Institute  
(ESRI), Menofia University, Sadat Branch, Sadat City, Egypt

K. Ocakoglu  
Advanced Technologies Research & Application Center, Mersin  
University, Ciftlikoy Campus, 33343 Mersin, Turkey

electrolyte, and catalyzes the reduction of triiodide ions. Therefore, counter electrode materials of high electrical conductivity and superior electrocatalytic activity are highly desired [8–10]. However, it is usually not easy to meet both the above requirements simultaneously.

Both of the PCBM (Phenyl-C61-butyrac acid methyl ester) and the P3HT (poly(3-hexylthiophene)) are qualified to be used as counter electrodes due to their higher carrier mobilities among the organic electronic materials. Moreover, the most intensively studied bulk heterojunctions are based on a PCBM and P3HT [11, 12].

The study of impedance spectroscopy for the conducting polymers is a powerful characterization tool to interpret the electron transport properties of the solar cells. Also, the impedance spectroscopy and its related parameters (capacitance, conductance and series resistance) at different biasing voltage and frequencies were used for modeling of frequency response of the fabricated dye-sensitized solar cells [13, 14]. In the present study, the PCBM:P3HT blend is deposited on the surface of FTO substrate as a new counter electrode for TiO<sub>2</sub>-based dye-sensitized solar cell using spin coating which is a low cost and easy technique. This work is focused on the fabrication and characterization of PCBM:P3HT/FTO nanostructure polymer counter electrode and its effectiveness on the photovoltaic performance as well as the conduction mechanism of fabricated DSSC. According to our knowledge, it is little work focused on the impedance spectroscopy and its related parameters (capacitance, conductance and series resistance) of the dye-sensitized solar cell at different biasing voltage and frequencies. Negative capacitance of the DSSC with the new PCBM/P3HT nanostructure counter electrode has been analyzed as a new phenomenon in a DSSC.

## 2 Experimental Procedures

### 2.1 Fabrication of Dye-Sensitized Solar Cell

#### 2.1.1 Preparation of TiO<sub>2</sub>/FTO Photoelectrode

Tetrabutyltitanate (10 mL) was rapidly added to distilled water (100 mL), a white precipitate was formed immediately. The precipitate was filtered using a glass frit and washed three times with 100 mL distilled water. The filter cake was added to nitric acid aqueous solution (0.1 M, 160 mL) under vigorous stirring at 80 °C until the slurry became a translucent blue-white liquid. The resultant colloidal suspension was autoclaved at 200 °C for 12 h to form white milky slurry. The resultant slurry was concentrated to one-fourth of its original volume, then PEG-20000 (10 wt% slurry) and a few drops of emulsification reagent of Triton X-100 were added to form a TiO<sub>2</sub> colloid.

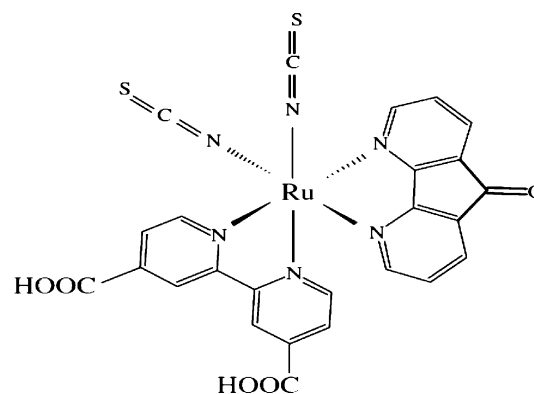


**Fig. 1** The chemical structure of K30 Ru dye

The TiO<sub>2</sub> colloid was dropped on the fluorine doped tin-oxide (FTO) glass plate using a doctor blading technique [15, 16]. The process was done for three times to form a thick TiO<sub>2</sub> film with about 9 μm. Finally, the TiO<sub>2</sub> porous film was sintered by firing the conducting glass sheet at 450 °C in air for 30 min. The K30 (Ru<sup>II</sup>(4,5-diazafluorene-9-one)(4,4'-dicarboxy-2,2'-bipyridyl) di(thiocyanate), [Ru<sup>II</sup>(L1)(H<sub>2</sub>dcby)(NCS)<sub>2</sub>]) dye (shown in Fig. 1) was used as a dye sensitizer in the fabricated DSSC [17]. The TiO<sub>2</sub>/FTO film electrode was immersed in an ethanolic solution of 2.5 × 10<sup>-4</sup> M K30 dye for 24 h to absorb the dye and then, the dye-sensitized TiO<sub>2</sub> film was washed up with anhydrous ethanol and dried in air atmosphere.

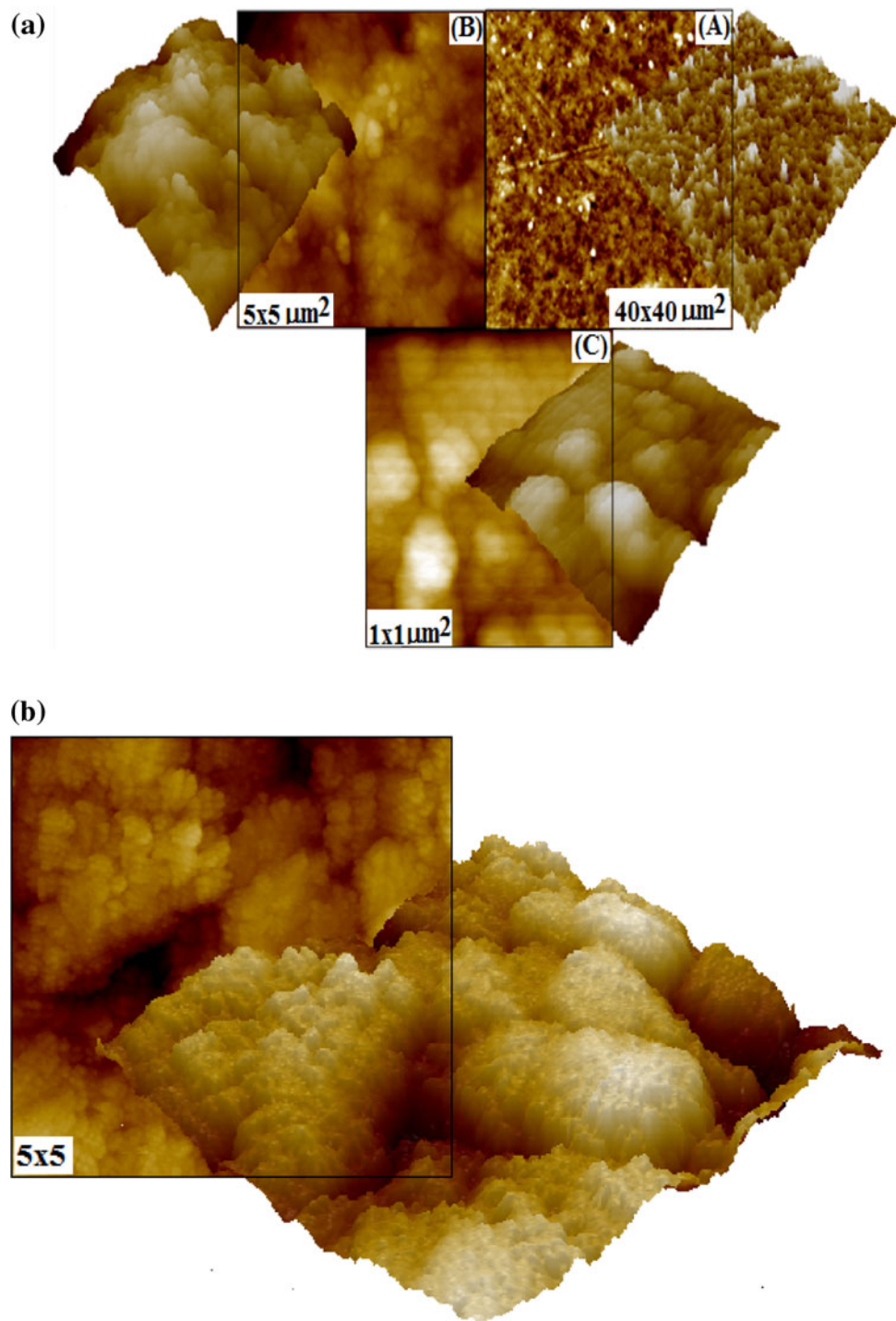
#### 2.1.2 Preparation of P3HT:PCBM/FTO Counter Electrode

[6,6]-Phenyl C61-butyrac acid methyl ester (PCBM) and poly(3-hexylthiophene) (P3HT) were purchased from Sigma–Aldrich Company. A solution of PCBM and P3HT (1:1 weight ratio) was prepared by stirring both PCBM and P3HT in chloroform for 1 h. The (P3HT:PCBM) blend thin film was deposited onto FTO coated glass using spin coating system model Xe-100. The deposited film of P3HT:PCBM onto FTO substrate was dried at 100 °C for 5 min in a tube furnace under N<sub>2</sub> flow.

#### 2.1.3 Assembling of FTO/TiO<sub>2</sub> + K30/PCBM:P3HT/FTO DSSC

The dye-sensitized solar cell was assembled by injecting the liquid iodide-triiodide electrolyte solution (0.5 M Lithium iodide mixed with 0.05 M iodine in water-free acetonitrile), into the aperture between the TiO<sub>2</sub> porous film electrode (anode electrode) and the (P3HT:PCBM) electrode (counter electrode). The two electrodes were clipped together and a cyanoacrylate adhesive was used as sealant to prevent the

**Fig. 2** **a** AFM micrographs of  $40 \times 40$ ,  $5 \times 5$  and  $1 \times 1 \mu\text{m}^2$  of PCBM:P3HT/FTO nano-structure counter electrode for the investigated DSSC. **b** 2D and 3D AFM images ( $5 \times 5 \mu\text{m}^2$ ) for  $\text{TiO}_2$  nano-clusters film of the investigated DSSC [18]



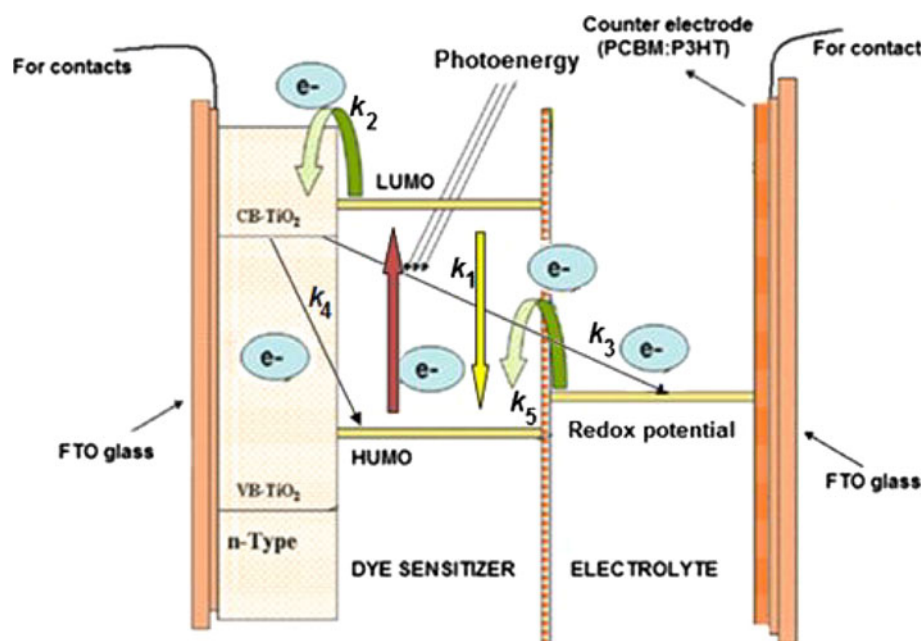
electrolyte solution from leaking. In addition to, an epoxy resin was used for further sealing the cell.

## 2.2 Measurements

The surface morphology of the nanostructure (P3HT:PCBM) counter electrode was investigated by atomic force

microscope (AFM, Park System, XE100) using a non-contact mode. The current–voltage characteristics under illuminations were measured using a KEITHLEY 4200-SCS semiconductor characterization system. The photovoltaic measurements were performed using a small-area class-BBA solar simulator and the light intensity was recalibrated by using (TM-206) solar power meter at different illumination levels.

**Fig. 3** Schematic energy diagram and operating principle for the investigated FTO/TiO<sub>2</sub> + K30/PCBM:P3HT/FTO DSSC



### 3 Results and Discussion

#### 3.1 Morphological Characteristics

Figure 2a shows the AFM images of PCBM:P3HT/FTO nanostructure counter electrode for the studied DSSC. 2D and 3D micrographs of ( $40 \times 40$ ,  $5 \times 5$  and  $1 \times 1 \mu\text{m}^2$ ) indicate that PCBM:P3HT blend has nano-clusters shape. The mean values of the nano-clusters sizes were found to be 104.466 nm for PCBM:P3HT blend. The roughness of 2D and micrographs of  $40 \times 40$ ,  $5 \times 5$  and  $1 \times 1 \mu\text{m}^2$  were found to be 53.921, 42.745 and 16.239 nm determined using a PARK system XEI software programming, respectively.

Figure 2b shows the 2D and 3D AFM images of TiO<sub>2</sub> nano-clusters of  $5 \times 5 \mu\text{m}^2$  thin film electrode of the fabricated DSSC. Both of the average roughness and the average nano-clusters size were determined to be 115.237 and 214.04 nm, respectively [18]. The TiO<sub>2</sub> spherical nanoparticles are well distributed and the film has a porous structure in which the nanoparticles were all bonded together through a sintering process. Such a porous structure permits not only the adsorption of a greater number of dye molecules, but also better wetting of the film by electrolyte. Together, these features result in a perfect penetration of the  $I^-/I_3^-$  redox couple into the TiO<sub>2</sub> film [19].

#### 3.2 Photovoltaic Characteristics

The functional diagram explaining the components of fabricated hybrid FTO/TiO<sub>2</sub> + K30/PCMB:P3HT/FTO

DSSC and dynamic process is shown in Fig. 3. The photovoltaic effect in DSSC occurs at the interface between a dye-anchored wide band gap oxide semiconductor and an electrolyte. The highest occupied molecular orbital (HOMO) of the dye molecules is usually formed by relatively weak lateral overlapping of atomic orbitals ( $\pi$  bonds) with loosely bond electrons ( $\pi$  electrons). Upon irradiation, the dye undergoes a  $\pi-\pi^*$  transition thereby exciting an electron to the lowest unoccupied molecular orbital (LUMO) of the dye ( $\pi^*$  electrons). The relaxation process of the excited electron into HUMO by constant rate ( $k_1$ ) is called nonradiative recombination. The injection of electrons into the conduction band (CB) of TiO<sub>2</sub> process is called interfacial electron transfer, in which the electrons are injected from the LUMO of the dye to the CB of TiO<sub>2</sub> photoelectrode with constant rate ( $k_2$ ). This interfacial electron transfer occurs typically in time scale of several picoseconds. Then, further transfer of electrons by capturing of the CB electrons into the oxidized species in the electrolyte with rate ( $k_3$ ) or the oxidized dye molecules with rate ( $k_4$ ) probabilities is called electron back transfer and interfacial charge recombination, respectively [20–22]. By rate ( $k_3$ ), the electron transfer from redox potential of the electrolyte to the HOMO of dye would move ahead by following the same first excitation process, leading to the transfer of electrons to the entire cell. During the entire cycle, the recovery of the holes is accomplished at the counter electrode. Among these processes, interfacial charge transfer is three orders of the magnitude faster than radiative recombination, i.e.,  $k_2/k_1 \approx 1000$ ; and electron back transfer is two orders of magnitude faster than interfacial charge recombination, i.e.,  $k_3/k_4 \approx 100$  [14].



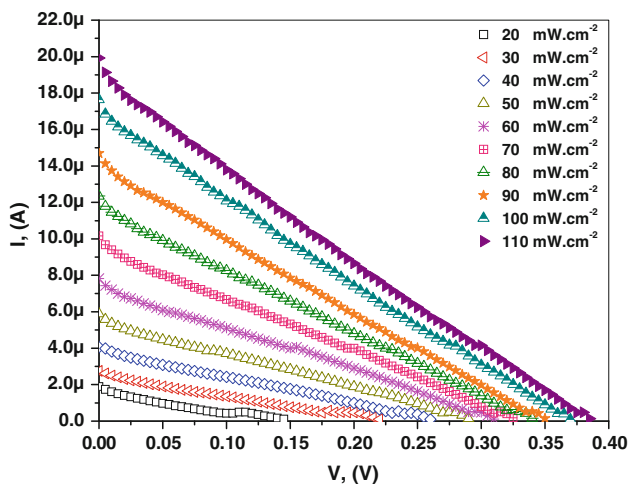


**Fig. 4** Plot of  $J-V$  curves for DSSC under different illumination intensities for investigated DSSC with PCBM:P3HT counter electrode

Therefore, it is reasonable to assume that these two factors i.e., radiative recombination and interfacial charge recombination, make negligible contribution to the final conversion efficiency [23, 24].

The photocurrent-voltage characteristics of the FTO/TiO<sub>2</sub> + K30/PCBM:P3HT/FTO DSSC under different illuminations light in the range 20–110 mW cm<sup>-2</sup> are shown in Fig. 4. As seen in Fig. 4, the solar cell shows a photovoltaic behavior with maximum open circuit voltage  $V_{oc}$  of 0.385 V and short-circuits current density  $J_{sc}$  of 0.163 mA cm<sup>-2</sup> under 110 mW cm<sup>-2</sup>. The increase of the photocurrent with increasing the light intensity can be attributed to the increasing in the electron conductivity of TiO<sub>2</sub> film due to electron injection from photosensitizers (K30 dye) under photon irradiation. In other words, with increasing the light illumination intensity, the injected electrons fill the trap site and/or surface levels in the TiO<sub>2</sub> film, the diffusion coefficient of the electron increase drastically, leading to elevated electron conductivity and good response of the photocurrent [25].

Figure 5 shows the relation between electrical power ( $P$ ) and bias voltage under different illuminations. It is clear that the electrical power increases with the biasing voltage until a maximum value and then it decreases to zero at the value of  $V_{oc}$  for each applied illumination. This maximum value is called the maximum power point with coordinate ( $P_{max} = I_{max} \times V_{max}$ ). Here,  $I_{max}$  and  $V_{max}$  are the maximum current and voltage values. The maximum power represents the condition where the solar cell can deliver its maximum power to the external load. The fill factor ( $FF$ ) measures the ideality of the device. In other words,  $FF$  is a measure of decrease in photocurrent with increasing the photovoltage and could be qualitatively determined from the squareness of the  $I-V$  curve and is

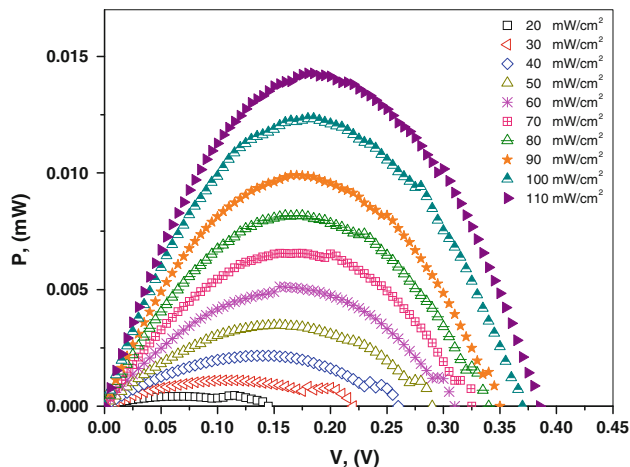


**Fig. 5** Plot of the output power versus voltage for investigated DSSC with PCBM:P3HT counter electrode

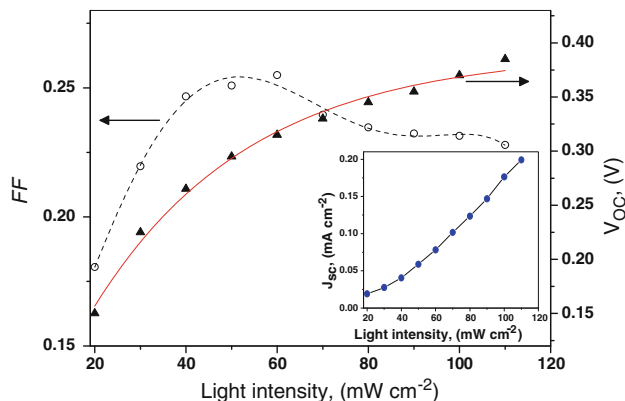


**Fig. 6** The effect of incident light intensities on  $FF$ ,  $V_{oc}$  and  $J_{sc}$  for the investigated DSSC. The solid lines represent the regression fitting and the dot line represents smoothing of the experimental data

defined as the ratio of the maximum electrical power to the product of  $I_{sc}$  and  $V_{oc}$  as follows:

$$FF = \frac{V_{max}I_{max}}{V_{oc}I_{sc}} \tag{1}$$

Figure 6 shows the dependence of the obtained values of  $FF$ ,  $V_{oc}$  and  $J_{sc}$  on the incident light intensity. Figure 6 declares that, the  $FF$  values increase with increasing of the light intensity until it reached to 0.255 under 60 mW cm<sup>-2</sup> illumination and then it is decreased which may be due to the ohmic losses in the cell [26]. The poor values of  $FF$  value (up to 0.255) can be attributed to the increase in the parallel current path such as electron back transfer ( $k_3$ ) and charge recombination ( $k_4$ ) within the device [27]. The values of  $V_{oc}$  increase with increasing the incident light intensity but the rate of this increasing becomes small after 60 mW cm<sup>-2</sup>. However,  $J_{sc}$  values grow exponentially with increasing in the incident light intensity up to

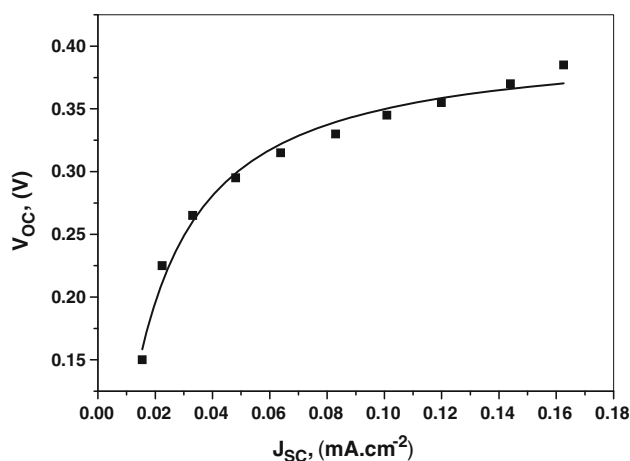


**Fig. 7** The variation of  $V_{oc}$  with  $J_{sc}$  for investigated DSSC with PCBM:P3HT counter electrode. The solid lines represent exponential fitting for the experimental data

$110 \text{ mW cm}^{-2}$  with the same rate. This increasing of  $J_{sc}$  indicates that both the photo-oxidization and regeneration (by the  $I^-/I_3^+$  ions) of the adsorbed K30 dye molecule are very efficient [26].

Figure 7 shows the results of varying the short circuit current density  $J_{sc}$  with the open circuit voltage  $V_{oc}$ . As seen from Fig. 7, that  $V_{oc}$  values increase exponentially with the increasing of  $J_{sc}$  values. The variation of  $V_{oc}$  with  $J_{sc}$  satisfying the following exponentially relation [25]:

$$V_{oc} = \ln \left[ \frac{I_{inj}}{qn_0k_{et}[I_3^-]} \right] \quad (2)$$

where  $I_{inj}$  is the flux of charge resulted from dye sensitization electron injection,  $q$  is the electron charge,  $n_0$  is the electron density on the CB of semiconductor in the dark,  $k_{et}$  is the constant rate of recombination reaction (between  $I_3^+$  and  $\text{TiO}_2$ ),  $[I_3^-]$  is the concentration of oxidized redox mediator  $I_3^-$  in the solution. This exponentially dependency of  $V_{oc}$  on  $J_{sc}$  satisfied that  $\eta\phi_0 \gg n_0k_{et}[I_3^-]$ , here  $\eta$  is the quantum yield for photogenerated electrons and  $\phi_0$  is the incident photon flux [28–32].

### 3.3 Impedance Spectroscopic Characteristics

The capacitance–voltage ( $C$ – $V$ ) characteristics for the studied  $\text{FTO}/\text{TiO}_2 + \text{K30}/\text{PCBM:P3HT}/\text{FTO}$  DSSC at different frequencies from 5 kHz to 1 MHz at the biasing voltage ( $-3$  to  $3$  Volt) are shown in Fig. 8. The variation of capacitance with voltage at the studied frequency range is characterized by two parts: positive values of capacitance with whole biasing voltage range (low frequency range,  $f \leq 100$  kHz), and negative capacitance with whole biasing voltage range in higher frequency range ( $f \geq 300$  kHz). However, at 200 kHz frequency the capacitance is varied

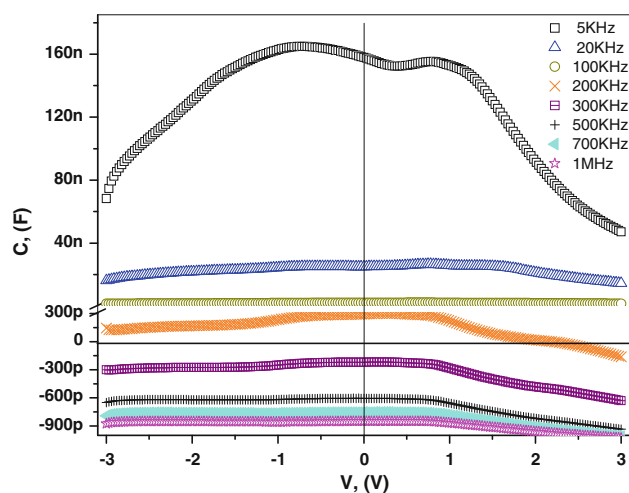


**Fig. 8** The frequency dependence of  $C$ – $V$  characteristics for investigated DSSC with PCBM:P3HT counter electrode measured at room temperature ( $RT$ )

from positive to negative values at biasing voltage ( $V > 2$  Volt). Here it worth to mentioning that, the negative capacitances (NC) were observed in several materials and it means that the material displays an inductive behavior, i.e., the current lags behind the voltage (current retardation) [33]. In fact, the NC phenomenon can be interpreted by means of a transient current analysis and can take place when: (i) the conductivity is inertial (i.e., the current lags behind the voltage) and (ii) the reactive component is larger than the displacement current [34]. Jonscher [35], Ershov et al. [36] and Wu et al. [37] reported that, the NC phenomenon is better viewed in the time domain. Upon the application of a positive voltage step, in a “normal” dielectric, the current decreases in time (polarization current) to eventually reach a constant value (dc conductivity). In that case, the capacitance is always positive in the frequency domain. On the contrary, at some times, the current increases and then, the capacitance could be negative in a certain range of frequencies. Appearance of NC in certain frequency domain has been attributed to several phenomena such as: carrier space charge limited currents [38], modification of traps population [39], carrier generation and recombination at interface states [40], injection through intermediate surface states [41] and modification of electronic barrier heights at grain boundaries (polycrystalline materials) or at junctions (diodes). Also, NC phenomena in metal–insulator–metal device [33] explained by a decrease in the Schottky barrier width at the metal–dielectric interface.

The real part of admittance ( $Y$ ) is presented in Fig. 9 in the form of the frequency dependence of the normalized conductance, i.e., conductance divided by the cyclic frequency. As seen in Fig. 9, the normalized conductance is decreased with increasing frequency in the whole range of

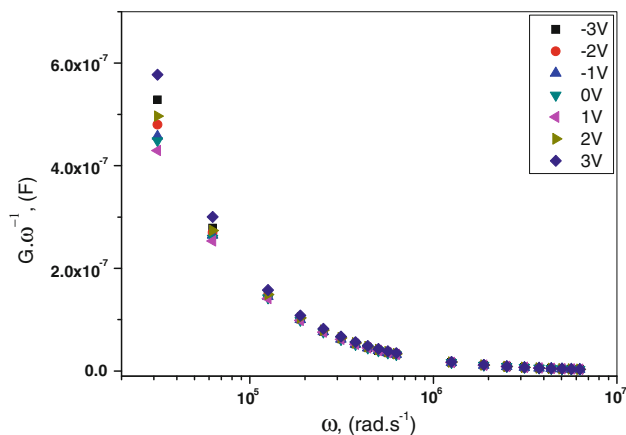


**Fig. 9** Frequency dependence of normalized conductance ( $G/\omega$ ) for investigated DSSC with PCBM:P3HT counter electrode measured at room temperature

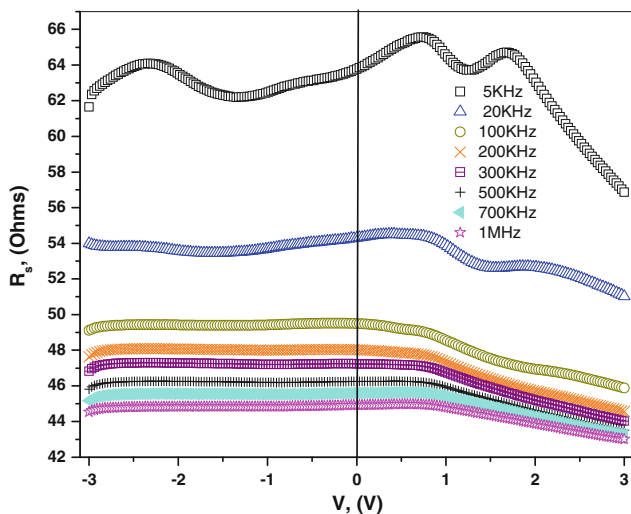


**Fig. 10** The frequency dependence of  $R_s$  versus  $V$  plot for investigated DSSC at room temperature

voltage, indicating that there is no response from any trap levels at room temperature [42].

The series resistance is an important parameter to determine the noise ratio of device in terms of frequency [43]. So, it is important to calculate the values of  $R_s$  at different voltage values for the whole investigated range of frequency. The frequency and voltage dependent series resistance of the device can be calculated from the experimental  $C-V-f$  measurements as [44]:

$$R_s = \frac{G_{ma}}{G_{ma}^2 + (\omega C_{ma})^2}, \quad (3)$$

where  $C_{ma}$  and  $G_{ma}$  are the measured values of capacitance and conductance, respectively. The series resistance of the investigated FTO/TiO<sub>2</sub> + K30/PCBM:P3HT/FTO DSSC

at different frequencies from 5 kHz to 1 MHz at biasing voltage (−3 to 3 Volt) is shown in Fig. 10. It is clear from Fig. 10, that the value of the series resistance values decrease systematically with increasing frequency.

#### 4 Conclusions

A new FTO/TiO<sub>2</sub> + K30 dye-sensitized solar cell with PCBM:P3HT/FTO counter electrode was fabricated. AFM micrographs confirmed the nanostructure form for both of the PCBM:P3HT/FTO counter electrode and the TiO<sub>2</sub> photoelectrode for the studied DSSC. The calculated photovoltaic parameters support the performance of DSSC using PCBM:P3HT counter electrode. Impedance spectroscopy including the capacitance–voltage ( $C-V$ ), conductance–voltage ( $G-V$ ), series resistances–voltage ( $R_s-V$ ) in a wide range of frequency were studied. The capacitance–voltage characteristics exhibit positive to negative capacitance, which represents a new phenomenon in DSSC which interpreted in details according to the basis of DSSC. The negative capacitance behavior may be attributed to different reasons such as: carrier space charge limited currents, modification of traps population, carrier generation and recombination at interface states, injection through intermediate surface states and modification of electronic barrier heights at grain boundaries.

**Acknowledgments** The authors (I.S. Yahia and Sh.A. Mansour) are grateful to the SCIENTIFIC AND TECHNOLOGICAL RESEARCH COUNCIL OF TURKEY (TUBITAK)–BIDEB for providing them by fellowships to work in Turkey via Research Fellowship Programme for Foreign Citizens.

#### References

1. B. O'Regan, M. Grätzel, *Nature* **353**, 737 (1991)
2. G.P. Smestad, *Sol. Energy Mater. Sol. Cells* **55**, 157 (1998)
3. M.K. Nazeeruddin, A. Kay, I. Rodicio, R. Humphry-Baker, E. Muller, P. Liska, N. Vlachopoulos, M. Gratzel, *J. Am. Chem. Soc.* **115**, 6382 (1993)
4. L.M. Peter, *Phys. Chem. Chem. Phys.* **9**, 2630 (2007)
5. Q. Qin, J. Tao, Y. Yang, X. Dong, *Polym. Eng. Sci.* **51**, 663 (2011)
6. F. Rodriguez, M.M. Castillo-Ortega, J.C. Encinas, H. Grijalva, F. Brown, V.M. Sanchez-Corrales, V.M. Castano, *J. Appl. Polym. Sci.* **111**,1216 (2009)
7. J. Han, Y. Liu, R. Guo, *J. Polym. Sci., Part A: Polym. Chem.* **46**, 740 (2008)
8. N. Papageorgiou, *Coord. Chem. Rev.* **248**, 1421 (2004)
9. J. Halme, M. Toivola, A. Tolvanen, P. Lund, *Sol. Energy Mater. Sol. Cells* **90**, 872 (2006)
10. J. Wu, Q. Li, L. Fan, Z. Lan, P. Li, J. Lin, S. Hao, *J. Power Sources* **181**, 172 (2008)
11. M.J. Panzer, D. Frisbie, *Adv. Funct. Mater.* **16**, 1051 (2006)
12. L. Chen, L. Yang, M. Shi, H. Chen, *Mater. Sol. Cells* **94**, 2244 (2010)

13. J.R. MacDonald, *Impedance Spectroscopy, Emphasizing Solid Materials and Systems* (Wiley, New York, 1987)
14. K. Lee, V. Suryanarayanan, K. Hoa, *J. Power Sources* **185**, 1605 (2008)
15. H. Hafez, J. Wu, Z. Lan, Q. Li, G. Xie, J. Lin, M. Huang, Y. Huang, M.S. Abdel-Mottaleb, *Nanotechnology* **21**, 415201 (2010)
16. H. Hafez, M. Saif, M.S.A. Abdel-Mottaleb, *J. Power Sources* **196**, 5792–5796 (2011)
17. K. Ocakoglu, C. Zafer, B. Cetinkaya, S. Icli, *Dyes Pigm.* **75**, 385–394 (2007)
18. I.S. Yahia, Hoda S. Hafez, F. Yakuphanoglu, B.F. Senkal, M.S. Abdel Mottaleb, *Synth. Met.* **161**, 1299–1305 (2011)
19. D. Kim, Y. Jeong, S. Kim, D. Lee, J. Song, *J. Power Sources* **149**, 112 (2005)
20. J. Ferber, R. Stangl, J. Luther, *J. Sol. Energy Mater. Sol. Cells* **53**, 29 (1998)
21. M. Grätzel, *J. Photochem. Photobiol. A* **164**, 3 (2004)
22. Md. K. Nazeeruddin, E. Baranoff, M. Graetzel, *Sol. Energy* **85**, 1172–1178 (2011)
23. M. Grätzel, *J. Photochem. Photobiol. C* **4**, 145 (2003)
24. J. Wu, Z. Lan, J. Lin, M. Huang, P. Li, *J. Power Sources* **173**, 585 (2007)
25. K. Hara, H. Arakawa, in *Handbook of Photovoltaic Science and Engineering* ed. by A. Luque, S. Hegedus (John Wiley, Sussex, 2003), pp.663–700
26. S. Wu, C. Chen, J. Chen, J. Li, Y. Tung, K. Ho, C. Wu, *Dyes Pigm.* **84**, 95 (2010)
27. R. Jose, V. Thavasi, S. Ramakrishna, *J. Am. Ceram. Soc.* **92**, 289 (2009)
28. K. Murakoshi, G. Kano, Y. Wada, S. Yanagida, H. Miyazaki, M. Matsumoto, S. Murasawa, *J. Electroanal. Chem.* **396**, 27 (1995)
29. M.K. Nazeeruddin, A. Kay, I. Rodicio, R. Humphry-Baker, E. Mueller, P. Liska, N. Vlachopoulos, M. Graetzel, *J. Am. Chem. Soc.* **115**, 6382 (1993)
30. A. Hagfeldt, M. Gratzel, *Chem. Rev.* **95**, 49 (1995)
31. Y. Huang, G. Schlichthörl, A.J. Nozik, M. Grätzel, A.J. Frank, *J. Phys. Chem. B* **101**, 2576 (1997)
32. A. Kumar, P. Santangelo, N. Lewis, *J. Phys. Chem.* **96**, 834 (1992)
33. F. El Kamel, P. Gonon, F. Jomni, B. Yangui, *Appl. Phys. Lett.* **93**, 042904 (2008)
34. G.B. Parravicini, A. Stella, M.C. Ungureanu, R. Kofman, *Appl. Phys. Lett.* **85**, 302 (2004)
35. A.K. Jonscher, *J. Chem. Soc., Faraday Trans. 2*, **82**, 75 (1986)
36. M. Ershov, H.C. Liu, L. Li, M. Buchanan, Z.R. Wasilewski, A.K. Jonscher, *IEEE Trans. Electron Devices* **45**, 2196 (1998)
37. X. Wu, E.S. Yang, H.L. Evans, *J. Appl. Phys.* **68**, 2845 (1990)
38. L.E. Byrum, G. Ariyawansa, R.C. Jayasinghe, N. Dietz, A.G.U. Perera, S.G. Matsik, I.T. Ferguson, A. Bezinger, H.C. Liu, *J. Appl. Phys.* **106**, 053701 (2009)
39. J. Bisquert, G.G. Belmonte, A. Pitarch, H.J. Bolink, *Chem. Phys. Lett.* **422**, 184 (2006)
40. F.A. Modine, R.B. Wheeler, Y. Shim, J.F. Cordaro, *J. Appl. Phys.* **66**, 5608 (1989)
41. F. Lemmi, N.M. Johnson, *Appl. Phys. Lett.* **74**, 251 (1999)
42. Y.Y. Proskuryakov, K. Durose, B.M. Tael, S. Oelting, *J. Appl. Phys.* **102**, 024504 (2007)
43. Sh.A. Mansour, F. Yakuphanoglu, *Solid State Sci.* **14**, 121–126 (2012)
44. E.H. Nicollian, J.R. Brews, *MOS Physics and Technology* (John Willey, New York, 1982)